JOURNAL OF GEOPHYSICAL RESEARCH, VOL. 103, NO. D6, PAGES 6043–6058, MARCH 27, 1998

Global sensitivity studies of the direct radiative forcing due to anthropogenic sulfate and black carbon aerosols

J. M. Haywood[1]
AOS Program, Princeton University, Princeton, New Jersey

V. Ramaswamy
Geophysical Fluid Dynamics Laboratory, Princeton University, Princeton, New Jersey

Abstract. The direct radiative forcing (DRF) of sulfate and black carbon (BC) aerosols is investigated using a new multispectral radiation code within the R30 Geophysical Fluid Dynamics Laboratory general circulation model (GCM). Two independent sulfate climatologies from chemical transport models are applied to the GCM; each climatology has a different atmospheric burden, vertical profile, and seasonal cycle. The DRF is calculated to be approximately -0.6 and -0.8 W m^{-2} for the different sulfate climatologies. Additional sensitivity studies show that the vertical profile of the sulfate aerosol is important in determining the DRF; sulfate residing near the surface gives the strongest DRF due to the effects of relative humidity. Calculations of the DRF due to BC reveal that the DRF remains uncertain to approximately a factor of 3 due to uncertainties in the total atmospheric burden, the vertical profile of the BC, and the assumed size distribution. Because of the uncertainties in the total global mass of BC, the normalized DRF (the DRF per unit column mass of aerosol in watts per milligram (W mg^{-1})) due to BC is estimated; the range is $+1.1$ to $+1.9$ W mg^{-1} due to uncertainties in the vertical profile. These values correspond to a DRF of approximately $+0.4$ W m^{-2} with a factor of 3 uncertainty when the uncertainty in the total global mass of BC is included. In contrast to sulfate aerosol, the contribution to the global DRF from cloudy regions is very significant, being estimated as approximately 60%. The vertical profile of the BC is, once again, important in determining the DRF, but the sensitivity is reversed from that of sulfate; BC near the surface gives the weakest DRF due to the shielding effects of overlying clouds. Although the uncertainty in the estimates of the DRF due to BC remains high, these results indicate that the DRF due to absorption by BC aerosol may contribute a significant positive radiative forcing and may consequently be important in determining climatic changes in the Earth-atmosphere system.

1. Introduction

Since preindustrial times, concentrations of atmospheric aerosols of anthropogenic origin appear to have increased [*Houghton et al.*, 1996]. These aerosols may influence the climate of the Earth via the direct effect by scattering and absorbing incident radiation [e.g., *Charlson et al.*, 1991; *Kiehl and Briegleb*, 1993; *Boucher and Anderson*, 1995; *Haywood et al.*, 1997a] and via the indirect effect by modifying the microphysical and optical properties of clouds [e.g., *Twomey*, 1977; *Jones et al.*, 1994; *Boucher and Lohmann*, 1995; *Jones and Slingo*, 1996]. Although the indirect effect may prove to exert a significant radiative forcing, this study concentrates solely upon the radiative forcing due to the direct effect.

Much recent work on the direct radiative forcing (DRF) of aerosols (i.e., the change in net irradiance at the top of the atmosphere due to the presence of aerosols [*Houghton et al.*, 1996]) has been focussed upon sulfate aerosol [e.g., *Charlson et al.*, 1991; *Kiehl and Briegleb*, 1993; *Boucher and Anderson*, 1995]. However, there is a growing realization that other aerosols of anthropogenic origin may exert a significant DRF and thus influence the climate of the Earth [*Houghton et al.*, 1996]. *Penner et al.* [1992] used a simple reflection model and neglected aerosol absorption to estimate the DRF due to biomass burning to be approximately -1 W m^{-2}. Recently, *Tegen et al.* [1996] estimated the DRF of anthropogenic sources of dust aerosol to be -0.25 W m^{-2} in the solar spectrum and $+0.34$ W m^{-2} in the terrestrial spectrum, resulting in a global net DRF of $+0.09$ W m^{-2}. *Haywood and Shine* [1995] assumed a global linear relationship between the mass of fossil-fuel black carbon (BC) and sulfate and used a simple reflection and absorption model to estimate the range of the DRF of fossil-fuel BC to be $+0.03$ to $+0.24$ W m^{-2}, depending upon the degree of internal and external aerosol mixing and the fractional mass of the BC. *Haywood et al.* [1997a] extended this study by using a general circulation model (GCM) and found the DRF due to fossil-fuel BC to be $+0.20$ W m^{-2} for an external mixture and $+0.36$ W m^{-2} for an internal mixture, assuming a BC/sulfate mass of 0.075. These results suggest a larger DRF from BC than the reflection and absorption model of *Haywood and Shine* [1995] because the GCM calculations include a significant DRF from BC that exists above and within clouds. It should be noted that neither *Haywood and Shine* [1995] nor *Haywood et al.* [1997a]

[1]Now at Met Research Flight, Meteorological Office, England.

Paper number 97JD03426.
0148-0227/98/97JD-03426$09.00

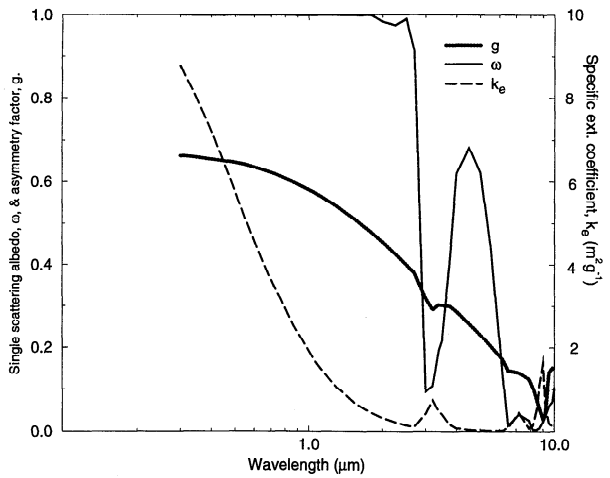

Figure 1. Specific extinction coefficient k_e, single scattering albedo ω, and asymmetry factor g for dry ammonium sulfate aerosol modeled by a lognormal distribution with a geometric mean radius of 0.05 μm and a geometric standard deviation of 2.0.

include the DRF of BC from biomass burning as global BC climatologies have only just become available. Only radiative forcings from sulfate and elemental carbon are investigated in this study. The emissions of organic carbon aerosols due to fossil-fuel and biomass burning are likely to produce a significant negative forcing [e.g., *Penner et al.*, 1992]; this radiative forcing is not examined in this study.

This study uses the new sulfate climatology of *Kasibhatla et al.* [1997] (KCS97) and the new BC climatology of *Cooke and Wilson* [1996] (CW96) to investigate the DRF due to sulfate and BC aerosols, respectively. Only anthropogenic sources of both types of aerosol are used in this study; natural emissions are not considered. Section 2 determines the radiative properties of both sulfate and BC by using Mie theory, and section 3 briefly describes the radiation code and the GCM that are used to determine the DRF. Section 4 presents the results for sulfate aerosol and includes calculations made using the sulfate climatologies of *Langner and Rodhe* [1991]. Section 5 presents the results for BC, and section 6 presents the results for an external mixture of the two aerosol species. A discussion and conclusions follow in section 7.

2. Aerosol Radiative Properties

The aerosol radiative properties are approximated throughout this study using Mie theory, the aerosol size distributions being modeled by lognormal distributions of the form [*WCP*, 1986]:

$$r\frac{dN}{dr} = \frac{N_0}{\ln \sigma \sqrt{(2\pi)}} \exp\left[-\left(\frac{(\ln r - \ln r_m)^2}{2(\ln \sigma)^2}\right)\right], \quad (1)$$

where r is the radius, N is the number of particles per unit volume with ln (radii) between ln (r) and ln (r) + d ln (r), N_0 is the total number density, r_m is the geometric mean radius, and σ is the geometric standard deviation.

Dry ammonium sulfate is modeled using a geometric mean radius of 0.05 μm and a geometric standard deviation of 2.0 [e.g., *Kiehl and Briegleb*, 1993; *Haywood et al.*, 1997a]. Base case calculations of the DRF due to BC are made assuming a geometric mean radius of 0.0118 μm and a geometric standard deviation of 2.0 [e.g., *World Climate Program* (*WCP*), 1986; *Haywood et al.*, 1997a]. The refractive indices for dry ammonium sulfate are from *Toon et al.* [1976], and a density of 1769 kg m^{-3} is assumed [*Weast*, 1987]. The refractive indices for BC are from *WCP* [1986]. Densities of BC in the literature vary from 625 kg m^{-3} for BC particles containing 75% empty space to 2250 kg m^{-3} for pure graphitic particles [*Horvath*, 1993]. Following *Haywood et al.* [1997a] and *Haywood and Shine* [1997], a density of 1000 kg m^{-3} is assumed, as this value gives a wavelength dependent specific extinction coefficient that is in agreement with many measurements [e.g., *Waggoner et al.*, 1976, 1981; *Horvath*, 1993].

The single scattering albedo ω, the asymmetry factor g, and the specific extinction coefficient k_e for dry ammonium sulfate and BC aerosols are shown in Figures 1 and 2, respectively. Figure 1 shows that the single scattering albedo for sulfate aerosol is unity throughout the majority of the solar spectrum, indicating that it acts to scatter incident solar radiation with no absorption. Figure 2 shows that the single scattering albedo for BC is less than 0.35 throughout the solar spectrum, indicating that BC absorbs a large fraction of the incident solar radiation. The specific extinction coefficient for both sulfate and BC is largest in the ultraviolet and visible regions of the spectrum but very small in the near infrared and thermal infrared, indicating a strong interaction with solar radiation but little interaction in the thermal infrared. Thus the DRF in the thermal infrared is a second-order effect [see *Haywood et al.*, 1997a] that is ignored in this study.

3. GCM Integrations

The R30 Geophysical Fluid Dynamics Laboratory (GFDL) GCM described by *Wetherald and Soden* [1995] is used to provide appropriate fields of gaseous species, surface reflectance, cloud, and solar insolation data. The spatial resolution is approximately 420 km by 250 km at the Equator, and there are 14 sigma levels in the vertical. A new 26-band two-stream δ-Eddington solar radiation scheme is included within the GCM [*Freidenreich and Ramaswamy*, 1997] that explicitly includes aerosol optical properties calculated from Mie theory and the cloud radiative properties parameterization of *Slingo* [1989]. This radiation code compares favorably against "refer-

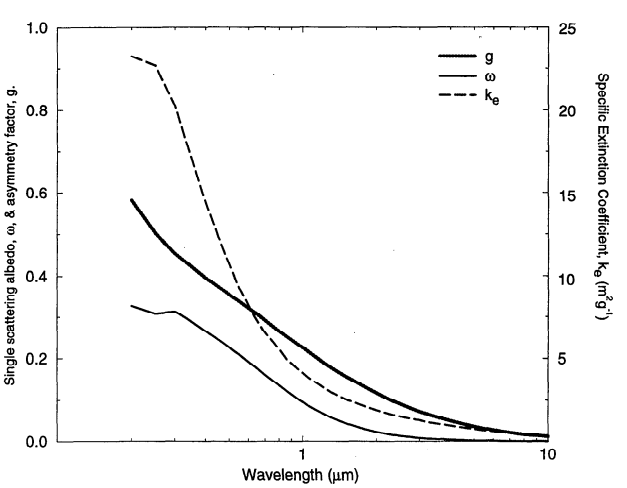

Figure 2. Specific extinction coefficient k_e, single scattering albedo ω, and asymmetry factor g for BC aerosol modeled by a lognormal distribution with a geometric mean radius of 0.0118 μm and a geometric standard deviation of 2.0.

ence" calculations performed with the line-by-line doubling and adding radiation code described by *Ramaswamy and Freidenreich* [1991]. When aerosol particles are present in cloudy regions of the atmosphere, an external mixture of cloud droplets and aerosol particles is assumed for both sulfate and BC aerosols. In the real atmosphere, some of the aerosols are likely to act as cloud condensation nuclei and become cloud droplets. This physical process is not included, as it is regarded to be a component of the indirect effect of aerosols, which is not considered in this study. The treatment of the aerosol and cloud droplets as an external mixture is unlikely to significantly affect the DRF because the contribution to the DRF from cloudy regions is found to be small (section 4.1).

The time step for the model integrations is 18 min for the dynamics, and the solar radiation scheme is called once every day. The radiative forcing is independent of ocean dynamics; therefore, only the atmospheric component of the GCM was integrated using observed seasonally varying sea surface temperatures. Cloud is assumed to exist throughout an entire grid box if the relative humidity exceeds a certain height-dependent threshold, the threshold ranging from 100% relative humidity in the lowest layer of the model to 90.15% in the highest model layer.

Three-dimensional monthly mean aerosol fields from KCS97 and CW96 are applied, and the DRF diagnostic is calculated as the difference between the top of the atmosphere net solar irradiance when the aerosol is excluded and when the aerosol is included. Thus the DRF in these calculations represents the instantaneous rather than the adjusted DRF [*Houghton et al.*, 1996]. These calculations use the average solar zenith angle in computing the DRF; the DRF obtained from the average solar zenith angle is weighted by the fractional day length to obtain the DRF diagnostic. The DRF will be a function of the diurnal variation of the solar zenith angle [e.g., *Pilinis et al.*, 1995; *Nemesure et al.*, 1995; *Haywood and Shine*, 1997; O. Boucher et al., Results from the Sulfate Shortwave Aerosol Radiative Forcing Intercomparison Project, submitted to *Journal of Geophysical Research*, 1997, hereinafter referred to as submitted paper]; this source of variation is ignored in this study. The atmospheric GCM is integrated for a period of 1 year, and monthly mean and annual mean diagnostics are computed. It is important to note that the effects of the aerosol upon the diabatic heating rates and, consequently, the dynamics of the model atmosphere are not included in computation of the DRF diagnostic. Coupled ocean-atmosphere model studies of the effects of sulfate aerosol upon global dynamics and climate have been performed by others [e.g., *Mitchell et al.*, 1995; *Meehl et al.*, 1996; *Haywood et al.*, 1997b] and are not discussed here.

4. Results: Sulfate Aerosol

Section 4.1 presents calculations for the base case, section 4.2 presents sensitivity calculations of the DRF to the relative humidity parameterization, and section 4.3 presents sensitivity calculations to the assumed vertical profile of the aerosol. Additional calculations using the *Langner and Rodhe* [1991] sulfate aerosol distributions are presented in section 4.4. The sensitivity of the DRF to the assumed sulfate size distributions and chemical composition has been investigated by others [*Kiehl and Briegleb*, 1993; *Boucher and Anderson*, 1995] and is not examined in this study.

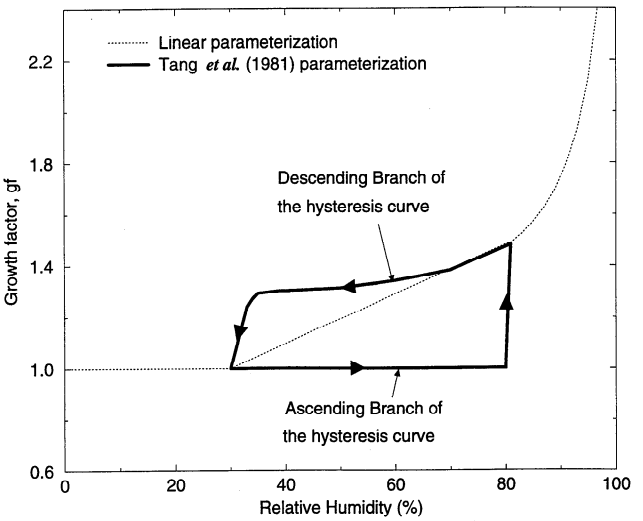

Figure 3. Growth factor gf for the linear, ascending, and descending relative humidity parameterizations described in the text.

4.1. Base Case Calculations

Sulfate is considered to be composed entirely of ammonium sulfate and is assumed to be hygroscopic. The relative humidity parameterization that accounts for the growth of sulfate aerosol particles with increasing relative humidity and the subsequent change in the aerosol optical properties is based upon the parameterization of *Fitzgerald* [1975] and is identical to the linear parameterization used by *Haywood et al.* [1997a] (see Figure 3).

Three-dimensional monthly mean aerosol anthropogenic sulfate fields from KCS97 are applied to the GCM; the annual mean column integrated sulfate burden is shown in Figure 4. As in many other modeling studies of the global sulfate distribution [e.g., *Langner and Rodhe*, 1991; *Pham et al.*, 1995; *Penner et al.*, 1994], there are three major peaks in sulfate distribution in the northern hemisphere occurring over the eastern United States, central and eastern Europe, and southeastern Asia. The average global column burden of sulfate is 1.76 mg m^{-2}, which is equivalent to a total atmospheric burden of 0.90 Tg SO_4^{2-}.

The annual mean DRF for the base case is shown in Figure 5. As expected from the sulfate distribution shown in Figure 4, the strongest DRF occurs in the three regions where the sulfate concentrations are high, results that are in agreement with several other modeling studies [e.g., *Kiehl and Briegleb*, 1993; *Boucher and Anderson*, 1995; *Haywood et al.*, 1997a]. The northern hemisphere DRF is -1.40 W m^{-2}, and the southern hemisphere DRF is -0.24 W m^{-2}, resulting in a global DRF of -0.82 W m^{-2}. These values are somewhat higher than the estimates of *Kiehl and Briegleb* [1993], *Boucher and Anderson* [1995], and *Haywood et al.* [1997a] but somewhat lower than the estimate of *Taylor and Penner* [1994].

The global mean normalized DRF (i.e., the forcing per unit column mass of sulfate in watts per milligram) is -0.46 W mg^{-1}. However, Figure 6 shows that the normalized DRF has a dramatic spatial variation and varies from approximately zero over areas of high surface reflectance such as the polar ice caps to -1 W mg^{-1} over oceanic regions near the equator. Similar results have been demonstrated in the detailed multispectral column calculations of *Haywood and Shine* [1997] and O. Boucher et al. (submitted paper, 1997). This is because the

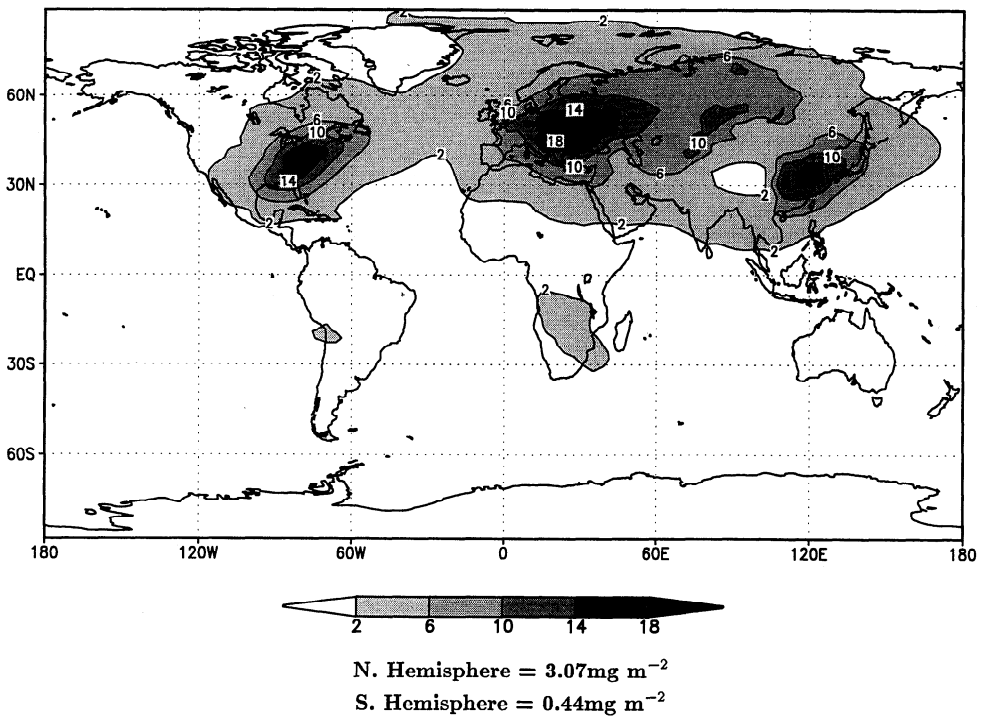

Figure 4. Total annual mean column burden of sulfate aerosol from the climatology of KCS97 (mg m^{-2}). The hemispheric mean column burdens are also shown.

normalized DRF is a strong function of surface reflectance, although solar irradiance, relative humidity, cloud optical depth and amount, and altitude of the aerosol also play a part in determining the normalized DRF.

It is possible to estimate the DRF from cloudy areas, ΔF_{cloud}, by adopting the cloud mask approach of *Haywood et al.* [1997a]. For each grid box, the monthly mean cloud amount A_c, the monthly mean DRF including clouds ΔF_{tot}, and the

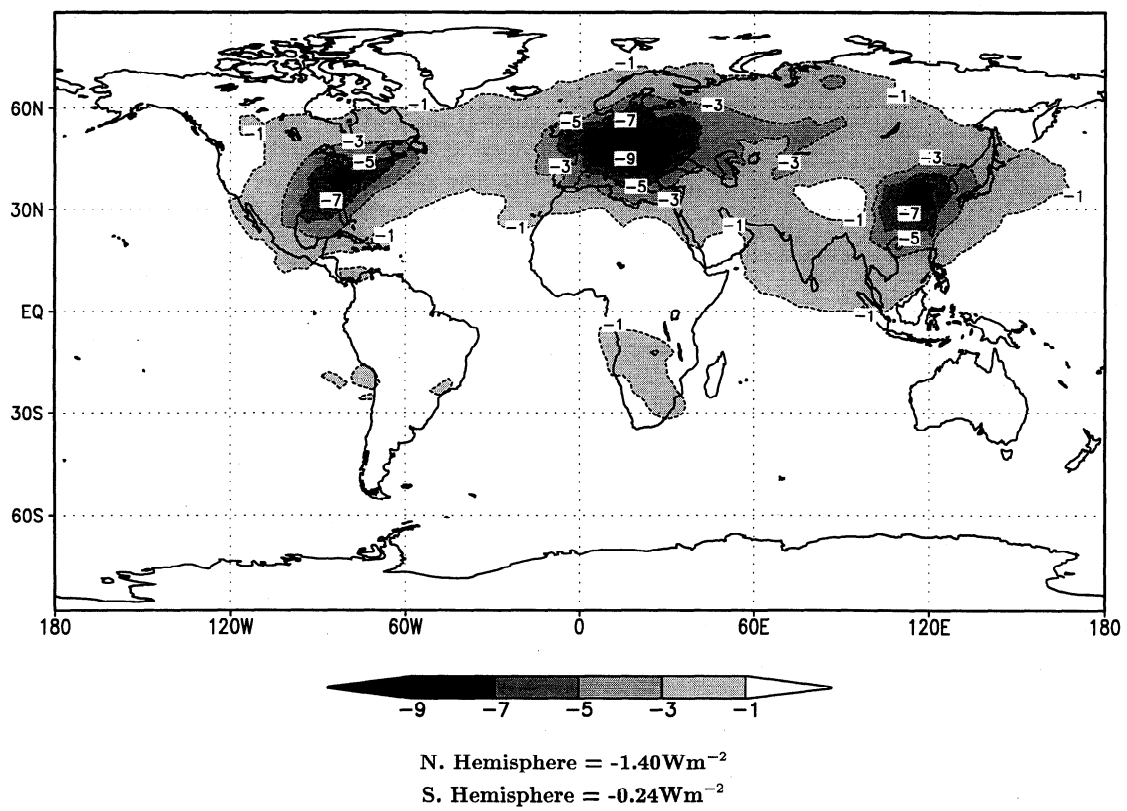

Figure 5. DRF due to sulfate aerosol using the climatology of KCS97 (W m^{-2}). The hemispheric mean DRFs are also shown.

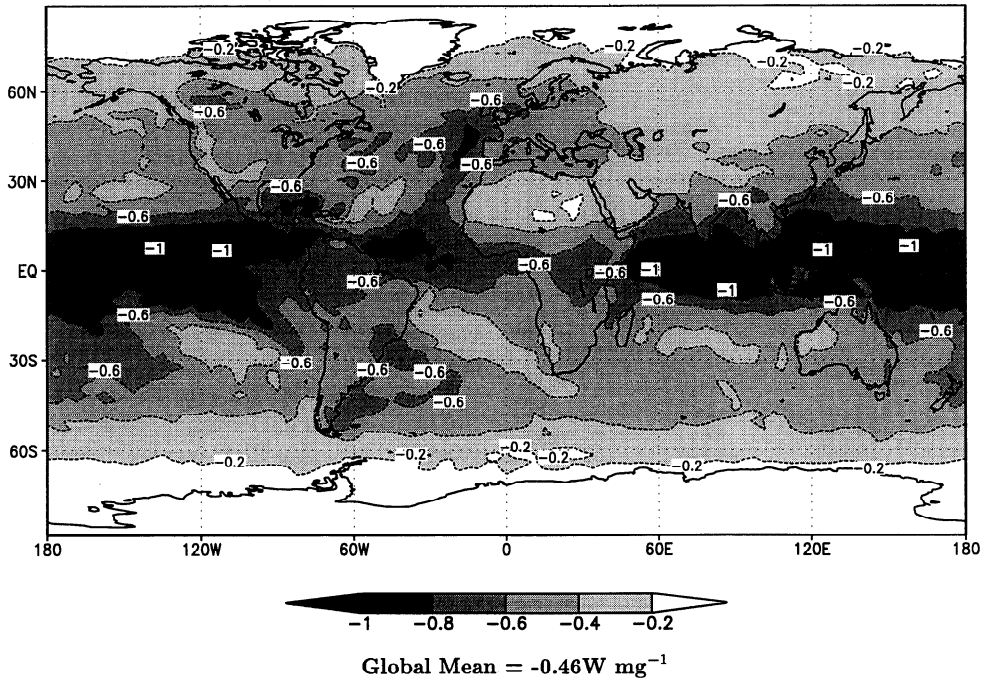

Figure 6. Normalized DRF due to sulfate aerosol using the climatology of KCS97 (W mg^{-1}). The global mean normalized DRF is also shown.

monthly mean DRF excluding clouds ΔF_{clear} are determined allowing calculation of ΔF_{cloud}. As shown by *Haywood and Shine* [1997], it is important to perform these calculations for each GCM grid box rather than using the bulk global values for DRF and cloud amount, as this allows for correlation between areas of strong DRF and clear-sky regions. The 12 monthly mean ΔF_{cloud} values are then used to calculate the annual ΔF_{cloud}. The results indicate that the contribution to the total global annual DRF from cloudy regions is approximately -0.09 W m^{-2}, or 11% of the total DRF. The results differ from those of *Boucher and Anderson* [1995], who neglected the spatial correlation between DRF and cloud and found a contribution to the total DRF from cloudy regions to be approximately 22%. They also differ from those obtained by *Haywood et al.* [1997a], who used an identical method to that described here and determined that the contribution of the DRF from cloudy skies to the total DRF was approximately 5%. The reasons for these differences are unclear but may be due to the fact that the *Haywood et al.* [1997a] calculations use a different cloud scheme and include a diurnal cycle. Once again, it should be noted that the sulfate aerosol and cloud droplets are considered to be an external mixture (section 3) and that the effect of sulfate particles upon cloud microphysical properties is not considered.

4.2. Investigations Into the Effects of Relative Humidity

In order to investigate the effects of relative humidity upon the DRF, seven additional 1-year model integrations were performed assuming the following.

1. The optical parameters for dry ammonium sulfate aerosol are without hygroscopic growth.

2. The optical parameters for ammonium sulfate are at a relative humidity of 70%. This relative humidity has been used in the study of *Haywood and Shine* [1995] in determining the DRF due to sulfate aerosol.

3. The optical parameters for ammonium sulfate are at a relative humidity of 80%. This relative humidity has been used in the study of *Charlson et al.* [1991] in determining the DRF due to sulfate aerosol.

4. The optical parameters for ammonium sulfate are at a relative humidity of 92%. As is shown below, this relative humidity gives a global DRF equal to that calculated in the base case (see Table 1).

5. The ammonium sulfate growth factor follows the ascending branch of the hysteresis curve of *Tang et al.* [1981] (see Figure 3).

6. The ammonium sulfate growth factor follows the descending branch of the hysteresis curve of *Tang et al.* [1981] (see Figure 3).

7. A single idealized subgrid-scale distribution of relative humidities is assumed that represents the distribution of relative humidities found in the model of *Haywood et al.* [1997c]. The distribution of relative humidities is assumed to be globally constant and is described by a triangular function with magnitude $\pm 10\%$ about the mean grid-box relative humidity for mean grid-box relative humidities below 90% (see distribution 1 in Figure 7). For mean grid-box relative humidities of over 90% the subgrid-scale relative humidity distribution is truncated at a relative humidity of 100% (see distribution 2 in Figure 7). This subgrid-scale relative humidity distribution is intended to represent that found in the limited-area nonhydrostatic model study of *Haywood et al.* [1997c], where the model simulates convection. In the real atmosphere the subgrid-scale distribution of relative humidities will vary globally and will not resemble that used here in many locations. It should also be noted that only the subgrid-scale effects of relative humidity are accounted for; no account is made for the subgrid-scale effects of cloud. However, this calculation is included to demonstrate the potential importance of subgrid-

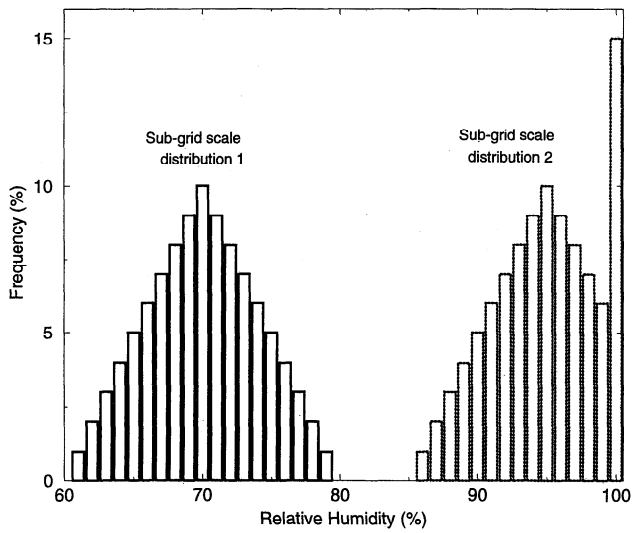

Figure 7. Diagram showing two possible subgrid-scale relative humidity distributions described in the text. The subgrid-scale parameterizations consist of simple triangular functions truncated at 100% relative humidity.

scale relative humidities in calculating the DRF. The results are summarized in Table 1.

Table 1 shows that the global DRF is the weakest at -0.31 W m^{-2} when no relative humidity growth is applied and the ammonium sulfate is considered to be dry. The global radiative forcing strengthens to -0.51 and -0.58 W m^{-2} when the optical parameters for moist aerosol at 70% and 80% relative humidities are used, respectively. These relative humidities have been used in estimating the DRF in models that do not include spatially varying relative humidities [e.g., *Charlson et al.*, 1991; *Haywood and Shine*, 1995]. Assuming that the aerosol relative humidity growth is best described by the hysteresis curve of *Tang et al.* [1981] leads to a global DRF of -0.76 W m^{-2} for the ascending branch of the hysteresis curve and -0.85 W m^{-2} for the descending branch of the hysteresis curve. These results indicate that the linear parameterization approach shown in Figure 3 should not lead to large inaccuracies in the calculation of the DRF.

The DRF is considerably stronger when the relative humidity fields from the R30 GCM are used than when an 80% constant relative humidity field is used because of the nature of the cloud scheme within the GCM. The cloud scheme consists of an on/off switch; clouds are included throughout the grid box if the relative humidity exceeds a certain height-dependent threshold relative humidity (see section 3). To demonstrate this, consider the lowest layers of the model, where the relative humidity threshold is approximately 100%. The global annual average relative humidity in the lowest layer of the model is 82%, but there are large spatial and temporal variations around this mean. Figure 3 shows that the increase in the growth factor at high relative humidities is very nonlinear, which in turn, leads to a DRF that also strengthens in a very nonlinear manner [e.g., *Haywood et al.*, 1997c]. As the R30 GCM does not form cloud in any one grid box until the relative humidity approaches 100%, relative humidities of 90–99.9% produce strong DRFs, and there is no cloud within the grid box to reduce the radiative forcing. Only when the relative humidity reaches 100% is cloud formed and the DRF in the grid box weakens dramatically, as the DRF is small in cloudy regions (see section 4.1). Thus, using the R30 GFDL model, a fixed relative humidity of 92% is necessary to obtain the same DRF as when the spatially varying relative humidity parameterization of the base case is used (see Table 1). GCMs that include a cloud fraction in each grid box in calculations of the DRF due to hygroscopic sulfate aerosol [e.g., *Boucher and Anderson*, 1995; *Haywood et al.*, 1997a] do not show such a high sensitivity to the inclusion of relative humidity parameterizations because, as the relative humidity increases in a grid box, so does the cloudy fraction. The nonlinearity of the DRF with increasing relative humidity and the moderating effect of cloud have been investigated in the limited-area model used by *Haywood et al.* [1997c].

The inclusion of a very simple idealized subgrid-scale relative humidity parameterization leads to the strongest DRF of -0.89 W m^{-2}, or a strengthening of approximately 9% when compared to the base case. *Haywood et al.* [1997c] showed that the subgrid-scale effects of relative humidity upon the DRF are reduced by the coexistence of cloud in areas of high relative humidity. To examine the extent of this cancellation, a model integration was performed excluding clouds from the model integration as in section 4.1. The global DRF is found to change from -1.64 W m^{-2} for the base case calculations excluding clouds and subgrid-scale relative humidity effects to -1.92 W m^{-2} when subgrid-scale effects are included, i.e., a strengthening of approximately 17%. As expected, this strengthening is of a larger magnitude than when clouds are included; these calculations indicate that the sensitivity to subgrid-scale variations in relative humidity when clouds are included is approximately half that of when clouds are excluded from the model integrations. It should be emphasized that a single global subgrid-scale relative humidity distribution is used in this study that is dependent only upon the mean relative humidity of the GCM grid box. No account is made for variations in the width or shape of the subgrid-scale distribution. To perform a more realistic global calculation of the effects of subgrid-scale variations in relative humidity and cloud would require a more sophisticated GCM parameterization and more accurate observations of both relative humidity and cloud amount.

4.3. Sensitivity of the DRF to the Vertical Profile of the Aerosol

It is interesting to investigate the sensitivity of the DRF to the vertical profile of sulfate aerosol, particularly as chemical transport models often rely on simplistic vertical transport mechanisms such as bulk parameterizations for deep convec-

Table 1. Variation of Direct Radiative Forcing for the Different Relative Humidity (RH) Schemes Described in the Text

Case	Northern Hemisphere	Southern Hemisphere	Global
Base case	−1.40	−0.24	−0.82
Dry	−0.52	−0.09	−0.31
70% RH	−0.86	−0.16	−0.51
80% RH	−0.99	−0.18	−0.58
92% RH	−1.39	−0.26	−0.82
Ascending	−1.30	−0.22	−0.76
Descending	−1.45	−0.25	−0.85
Subgrid RH	−1.52	−0.25	−0.89

Unit of measure is W m^{-2}.

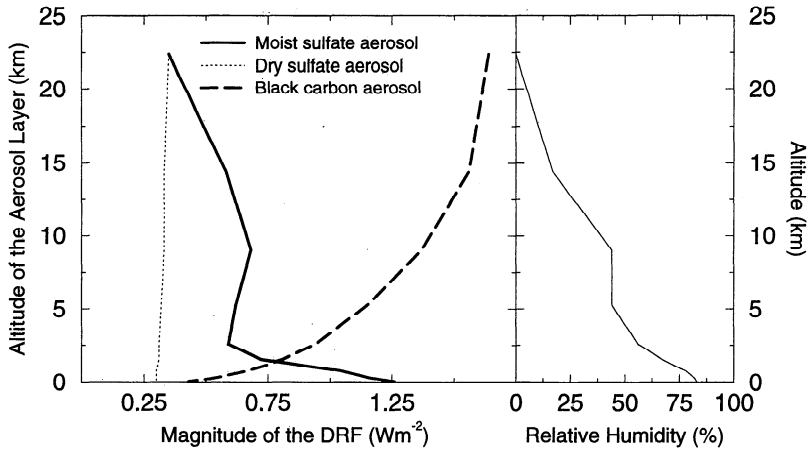

Figure 8. Sensitivity of the DRF (W m^{-2}) to the altitude of the aerosol layer within the GFDL R30 GCM. Plots are shown for dry ammonium sulfate, moist ammonium sulfate using the linear relative humidity parameterization scheme shown in Figure 3, and BC aerosol. Note that the magnitude of the radiative forcing is shown and that the DRF due to sulfate aerosol is actually negative. The global annual mean relative humidity at each model level is also shown.

tive processes, leading to large uncertainties in the vertical profile of the aerosol. Additionally, the scarcity of measurements at different altitudes means that the global distribution of the vertical profile of sulfate aerosol is not well known. To investigate the sensitivity of the DRF to changes in the vertical profile of the sulfate aerosol, the following method was applied. The monthly mean column integrated dry sulfate mass was determined and applied, in turn, to a single layer of the GCM. GCM calculations of the annual DRF were performed both for dry ammonium sulfate and assuming the linear relative humidity parameterization of the base case. The results are shown in Figure 8.

Figure 8 shows that the DRF is a strong function of the altitude of the aerosol when the linear relative humidity parameterization used in the base case is applied, the DRF being strongest when the sulfate aerosol layer is nearest to the surface. The DRF weakens by approximately a factor of 2 as the altitude of the aerosol layer is raised to 2.5 km. As the aerosol layer is raised above 2.5 km, the DRF strengthens with altitude up to approximately 9 km before weakening again as the sulfate is moved to higher altitudes. These effects can be explained by considering the effects of relative humidity. When the aerosol layer is near the surface of the Earth, the global mean relative humidity is high at approximately 82%, leading to a large growth factor, a correspondingly large specific extinction coefficient, and hence a strong DRF. As the aerosol layer moves up to 2.5 km altitude, the global mean relative humidity decreases, leading to a decrease in the DRF. As the aerosol layer is moved to higher altitudes, the GCM relative humidity remains approximately constant up to 9 km, and there is a small strengthening in the DRF because there is less scattering and absorbing atmosphere above the aerosol; hence there is more solar radiation incident upon the aerosol. The subsequent decrease in the relative humidity with altitude leads to decreases in the DRF until the DRF is identical to that for dry ammonium sulfate aerosol at altitudes of approximately 22 km. It is interesting to note that the parameterization for hygroscopic growth with increasing relative humidity has a threshold relative humidity of 30%; therefore one might expect that the DRF for moist aerosol might be equal to that for dry aerosol above altitudes of approximately 14 km. However, there are significant spatial and temporal variations in the model relative humidity at this level, which frequently exceeds 90%, leading to large differences in the DRF for moist and dry aerosol even at high altitudes. Thus, as in the case for spatial subgrid-scale variations in relative humidity, temporal variations of the relative humidity are also important in determining the DRF. It should be noted that although the relative humidity profile of the R30 GCM may not be representative of the real atmosphere at every location, many of the relative humidity profiles of *McClatchey et al.* [1972] show the same general features as the annual global mean profile shown in Figure 8.

4.4. Application of the *Langner and Rodhe* [1991] Sulfate Climatology

To investigate the effects of applying another sulfate climatology, the "slow oxidation" climatology of *Langner and Rodhe* [1991] (LR91) is used in place of the climatology of KCS97. This sulfate distribution has been used previously in the studies of *Kiehl and Briegleb* [1993] and *Haywood et al.* [1997a], although *Haywood et al.* [1997a] used the annual mean distribution rather than the monthly mean distributions.

The spatial pattern of the annual mean distribution of LR91 strongly resembles that of KCS97, with peak sulfate concentrations over the eastern United States, central Europe, and southeastern Asia. Additionally, the annual mean sulfate burdens from LR91 are 1.83 mg m^{-2} globally, 3.08 mg m^{-2} for the northern hemisphere, and 0.60 mg m^{-2} for the southern hemisphere, showing good quantitative agreement when comparing against the burdens from KCS97 shown in Figure 4. However, the seasonal cycle of the sulfate burdens differ, with the LR91 data showing maximum northern hemisphere concentrations in February and the KCS97 data showing two peaks in February and September (see Figure 9).

Three model integrations are performed using the LR91 data in place of KCS97 data; the first corresponds to the base case performed in section 4.1, the second to the dry case performed in section 4.2, and the third uses fixed optical parameters for sulfate aerosol at 80% relative humidity. The results are summarized in Table 2.

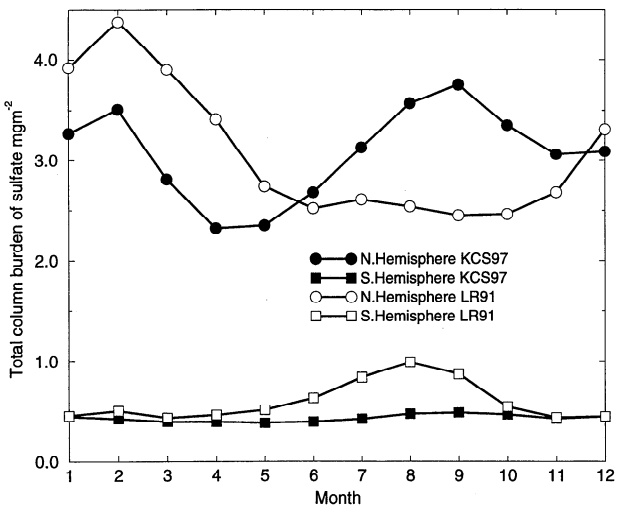

Figure 9. Seasonal cycle of the hemispheric mean column burden of sulfate aerosol (mg m^{-2}) for KCS97 and for LR91.

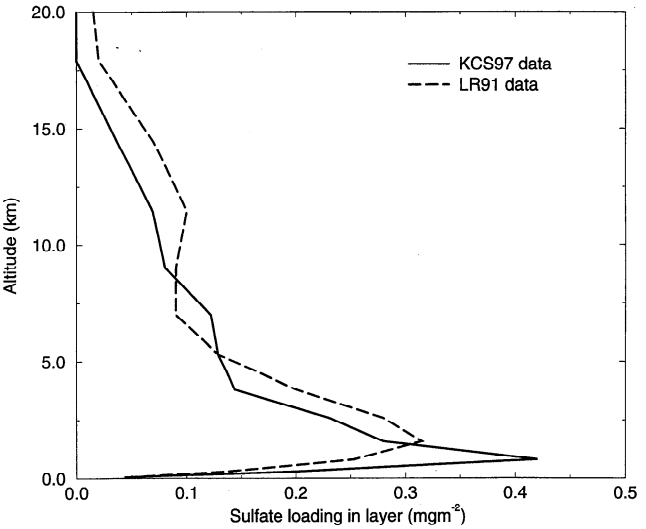

Figure 10. Sulfate loading in each layer of the R30 GFDL model. Vertical profiles for both KCS97 and LR91 are shown.

Table 2 shows that, for the base case, the DRF for LR91 is 23% lower than for KCS97 but for the other two cases the DRF for LR91 is only 5% lower than for KCS97. The DRF is weaker for LR91 in the dry and 80% relative humidity cases due to a combination of effects including differences in the seasonal cycle, differences in the model relative humidity profile, and differences in the spatial distribution of the aerosol. The larger difference in the base case calculations can be explained by considering differences in the vertical profile of the aerosol. The annual mean mass of sulfate in each layer of the GCM for the KCS97 and LR91 climatologies is shown in Figure 10. Although the vertical profiles are similar with a peak in the lower troposphere and a general decrease with altitude, the peak in the LR91 data is at a higher altitude than the KCS97 data, and the mass of sulfate in the lower layers of the GCM is lower. Thus the LR91 data have less sulfate aerosol at higher relative humidities (see Figure 8), and the sensitivity of the DRF to inclusion of a relative humidity parameterization will therefore be lower (see section 4.3). These results emphasize that the vertical profile of the sulfate aerosol produced by the chemical transport models needs to be accurate if estimates of the DRF due to hygroscopic aerosols such as sulfate are to be improved. Accurate representation of the vertical profile of the aerosol may require improved vertical resolution to reduce the effects of artificial diffusion which may result in displacement of aerosol mass to higher altitudes.

It is also worth considering how differences in the seasonal cycle of the sulfate aerosol shown in Figure 9 affect the seasonality of the DRF. The hemispheric seasonal cycles of the DRF for LR91 and KCS97 are shown in Figure 11 for the base case calculations for each aerosol climatology. In the northern hemisphere the DRF for LR91 has a broad peak in April–July, and the DRF for KCS97 has a broad peak in June–September. Note that in February and April the northern hemisphere DRF is similar for the two sulfate data sets despite the fact that the sulfate burden is higher in LR91 than in KCS97 in these months (see Figure 9) due primarily to differences in the vertical profile and the effects of relative humidity. From these calculations it appears that the northern hemisphere DRF due to sulfate peaks in the summer months because of the additional insolation regardless of the seasonal cycle of the sulfate burden, although the strongest DRF is delayed from May for LR91 to August for KCS97.

Table 2. Global Mean Direct Radiative Forcing for Using Sulfate Climatologies of KCS97 and LR91

Case	*Kasibhatla et al.* [1997]	*Langner and Rodhe* [1991]
Base case	−0.82	−0.63
Dry	−0.31	−0.29
80% RH	−0.58	−0.56

RH, relative humidity. Unit of measure is W m^{-2}.

5. Results: Black Carbon Aerosol

As in the case of sulfate aerosol, the optical properties of BC aerosol were determined using Mie theory applied to a log-normal size distribution (see section 2). BC is considered to be

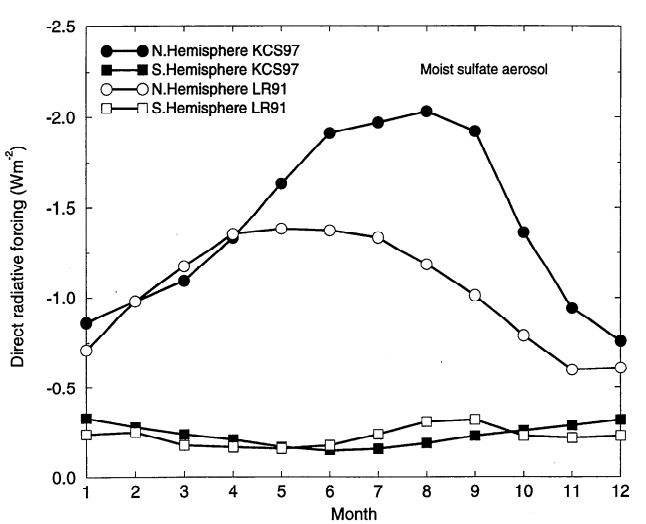

Figure 11. Seasonal cycle of the hemispheric mean DRF (W m^{-2}) for KCS97 and for LR91.

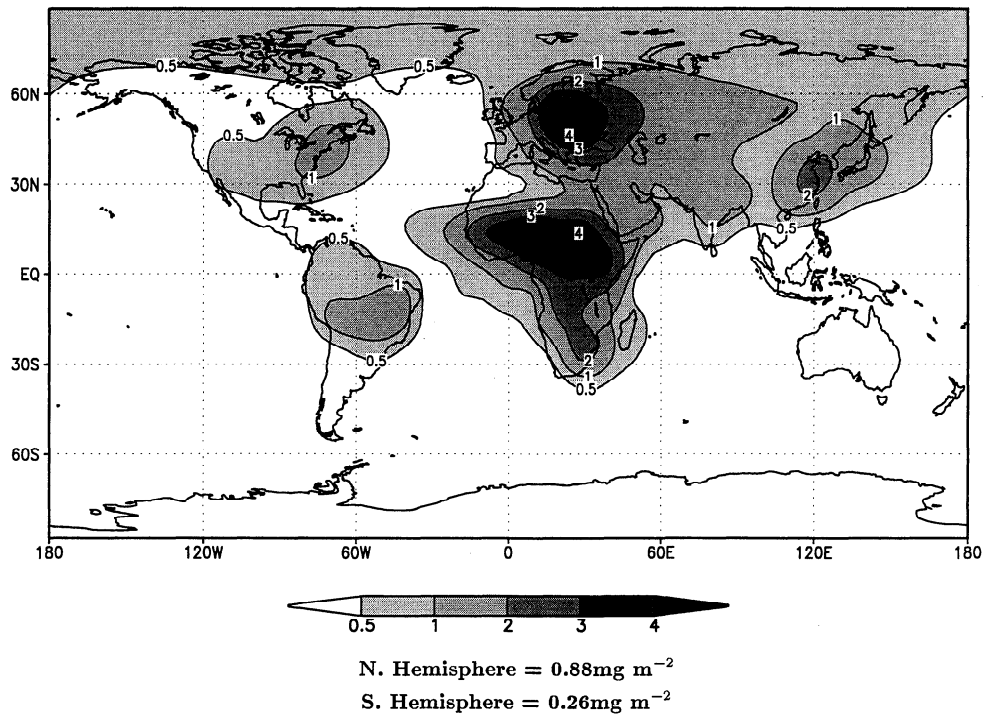

Figure 12. Total annual mean column burden of BC aerosol from the BC climatology of CW 96 (mg m^{-2}). The hemispheric mean column burdens are also shown.

hydrophobic throughout this work [*Horvath*, 1993], although *Parungo et al.* [1992, 1994] suggest that BC may become coated with sulfate aerosol from fossil-fuel emissions subsequent to emission. Recent global modeling studies also suggest that BC becomes hygroscopic as it ages due to mixing with other aerosol particles, resulting in internal aerosol mixtures [e.g., *Liousse et al.*, 1996; CW96]. Section 5.1 presents base case calculations, section 5.2 examines the effects of different size distributions, section 5.3 examines the effect of different vertical profiles, and section 5.4 presents calculations of the normalized DRF.

5.1. Base Case Calculations

The monthly mean BC climatologies from CW96 were applied to the R30 GCM. The annual mean global BC burden from the CW96 data is shown in Figure 12, which shows peaks similar to those for sulfate aerosol and, in addition, significant peaks in BC column burden in Africa and South America. This is because the BC climatology of CW96 includes emissions of BC from industrial regions of the northern hemisphere and, in addition, emissions from biomass burning. The annual mean column burden of BC is 0.57 mg m^{-2}, which is equivalent to a total atmospheric burden of approximately 0.28 Tg.

The global mean DRF from BC for the base case is shown in Figure 13. The northern hemisphere mean DRF is +1.70 W m^{-2}, and the southern hemisphere mean DRF is +0.42 W m^{-2}, resulting in a global mean DRF of +1.06 W m^{-2}. The largest DRF occurs over regions of central Africa, eastern Europe, southeast Asia, and the Himalayas.

The global mean normalized DRF (i.e., the forcing per unit column mass of BC) is +1.85 W mg^{-1}, but as in the case for sulfate aerosol, the normalized DRF varies widely spatially, with normalized DRFs ranging from approximately zero over ocean areas of low surface albedo in the tropics to 5 W mg^{-1} over highly reflectant ice sheets (Figure 14). The specific extinction coefficient at 0.55 μm for dry sulfate is approximately 5.0 m^2 g^{-1}, while that for BC aerosol is 9.3 m^2 g^{-1} (see Figures 1 and 2). As seen in section 4.2, a fixed relative humidity of 92% is required to reproduce the global annual mean radiative forcing of the sulfate aerosol base case. The specific extinction coefficient for sulfate aerosol at 92% relative humidity is approximately 20 m^2 g^{-1}; thus the mean specific extinction coefficient for hydrated sulfate aerosol is approximately double that of BC aerosol. Thus it is interesting that the normalized DRF is much larger for BC aerosol than for hydrated sulfate aerosol even though the specific extinction coefficient is a factor of 2 lower. The reasons for the higher sensitivity of the normalized DRF of BC are twofold. First, the DRF is not solely a function of the specific extinction coefficient but a function of the surface albedo. According to *Chylek and Wong* [1995], the DRF in clear skies of a partially absorbing aerosol may be approximated in a simple reflection absorption model by

$$\mathrm{DRF} \approx -\frac{S_0}{4} T_{\mathrm{at}}^2 (1 - A_c)[(1 - R_s)^2 2\beta\tau_{\mathrm{sca}} - 4R_s\tau_{\mathrm{abs}}] \qquad (2)$$

where S_0 is the solar constant, T_{at} is the transmission of the atmosphere above the aerosol layer, A_c is the cloud amount, R_s is the surface reflectance, β is the backward scattered fraction, τ_{sca} is the scattering optical depth, and τ_{abs} is the absorption optical depth. We consider two simplified aerosols each of identical optical depth but one which purely scatters radiation ($\tau_{\mathrm{abs}} = 0$), giving rise to $\mathrm{DRF}_{\mathrm{sca}}$, and one which purely absorbs incident radiation ($\tau_{\mathrm{sca}} = 0$), giving rise to $\mathrm{DRF}_{\mathrm{abs}}$. Application of a global mean R_s of 0.15 [e.g., *Charlson et al.*, 1991] and a β of 0.21 [*Kiehl and Briegleb*, 1993] leads to

$$\mathrm{DRF}_{\mathrm{abs}} \approx 2 \times \mathrm{DRF}_{\mathrm{sca}} \qquad (3)$$

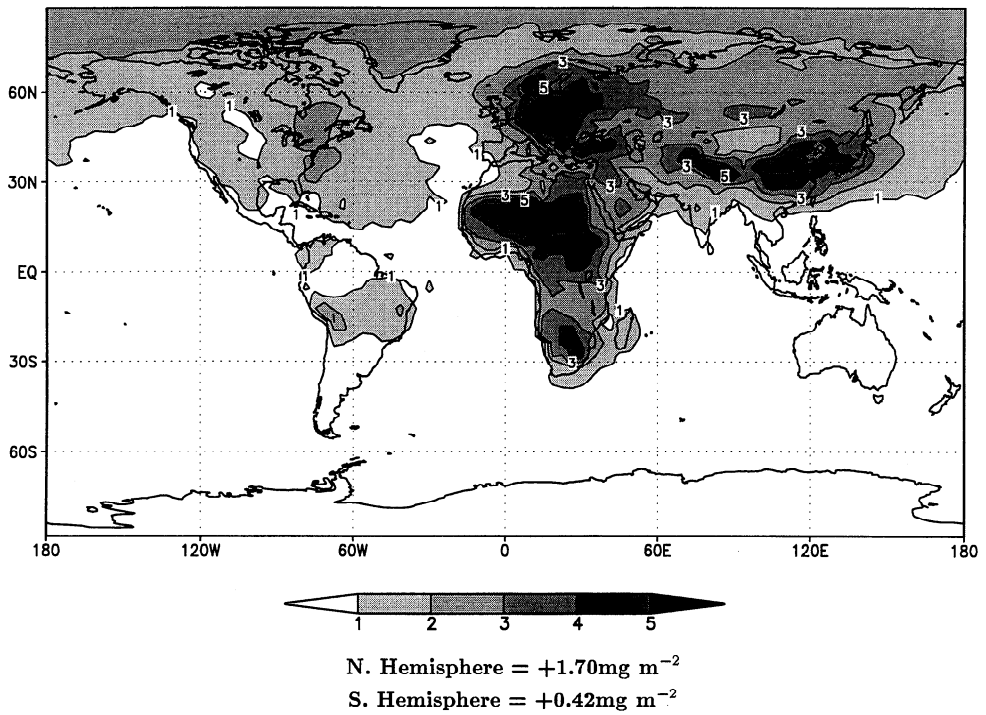

Figure 13. DRF due to BC aerosol using the climatology of CW96 (W m^{-2}). The hemispheric mean DRFs are also shown.

Thus the absorbing aerosol will produce a clear-sky DRF that is approximately double that for the scattering aerosol. Therefore, in our analysis where the specific extinction coefficient for sulfate is approximately double that for BC, one might expect the normalized clear-sky DRF to be similar in both cases. Calculations reveal that the normalized clear-sky DRF is approximately +1.16 W mg^{-1} for BC and −0.99 W mg^{-1} for sulfate aerosol, indicating the approximate validity of the argument outlined above.

The second reason for the stronger DRF due to BC is that whereas sulfate aerosol exerts a reduced DRF in cloudy regions (section 4.1), the DRF due to BC in cloudy regions is amplified [e.g., *Haywood and Shine*, 1997; *Haywood et al.*, 1997a] (see section 5.3). This is because the presence of

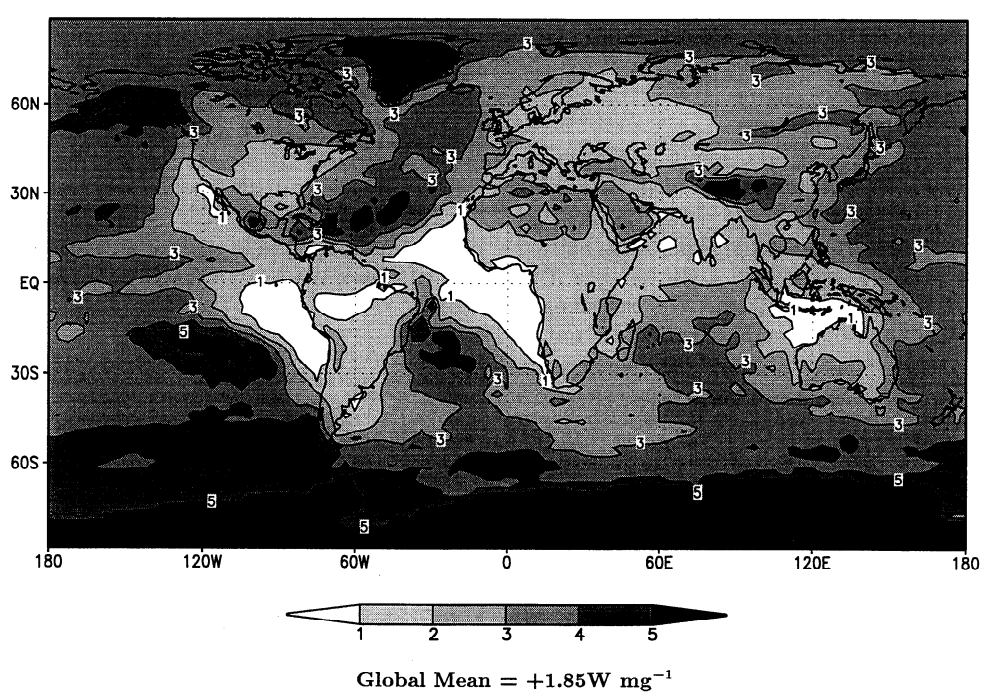

Figure 14. Normalized DRF (W mg^{-1}) due to BC aerosol using the climatology of CW96. The global mean normalized DRF is also shown.

strongly absorbing BC above highly reflective cloud has a much larger effect upon the planetary albedo than the same amount of BC over a less reflectant surface. This may be demonstrated using an identical cloud-masking procedure to that for sulfate aerosol. Application of this method reveals a contribution from cloudy regions of +1.00 W m^{-2} for the northern hemisphere and +0.27 W m^{-2} from the southern hemisphere, yielding a global contribution from the cloudy regions of approximately +0.64 W m^{-2}. Thus the contribution from cloudy regions is over 60% of the total DRF. This sensitivity is radically different from the results for sulfate aerosol where the contribution from the cloudy regions was found to be 11% of the total DRF. It should be noted that BC is considered to be hydrophobic throughout the study, and it is modeled as an external mixture when it coexists with cloud droplets. In the recent study of *Chylek et al.* [1996], approximately 9% of the in-cloud BC was found to exist internally mixed with cloud droplets. The radiative effects of such internal mixtures are likely to lead to a more positive DRF than a corresponding external mixture of the same chemical composition [e.g., *Chylek et al.*, 1984, 1988; *Fassi-Fihri et al.*, 1997].

5.2. Sensitivity to the Assumed Size Distribution

Just as the sulfate climatologies of KCS97 and LR91 do not contain any information about the size distribution of sulfate within the atmosphere, the BC climatology of CW96 does not contain any information on the size of the BC particles. Sulfate aerosol however, is formed from the precursor gas sulfur dioxide via gaseous and aqueous phase reactions (e.g., LR91), whereas BC is emitted directly by the combustion source. BC may be emitted over a wide range of size distributions, depending upon the combustion source and the type of combustion. Subsequent to emission, coarse particles may fractionate into fine particles or be removed from the atmosphere via sedimentation; thus the atmospheric lifetime of coarse BC is short, leading to local and regional rather than global-scale transport. At least two distinct size distributions of BC aerosol particle have been observed in the atmosphere corresponding to fine- and coarse-mode particles [e.g., *Berner et al.*, 1996]. In modeling studies, *WCP* [1986] assume a geometric mean radius of 0.0118 μm, a value that is adopted in the base case calculations detailed in section 5.1. However, *Shettle and Fenn* [1979] model coarse BC particulates in urban/industrial regions with a geometric mean radius of 0.50 μm. Both of these models assume that the geometric standard deviation of the size distribution is 2.0.

A definitive segregation of the CW96 BC climatology into coarse- and fine-mode particles is difficult; therefore a sensitivity study spanning the fine and coarse particle size distributions is performed. The results are shown in Table 3.

Table 3 shows that the DRF is a very strong function of the assumed geometric mean radius of the aerosol distribution, with the global DRF ranging from +1.06 W m^{-2} for fine-mode BC with a geometric mean radius of 0.01 μm, dropping to +0.15 W m^{-2} for a coarse-mode BC with a geometric mean radius of 0.5 μm, thus highlighting the need for size discretization in chemical transport models.

5.3. Sensitivity of the DRF to the Vertical Profile of the Aerosol

A similar method to that outlined in section 4.3 was pursued using the optical properties of BC in place of the optical properties of sulfate and the monthly mean BC climatologies in place of the sulfate climatologies. Figure 8 shows that the DRF for BC is largest when the aerosol is placed at high altitudes in the GCM and is smallest when the aerosol is at low altitudes. Comparison with the sulfate DRF shows that the variation is less complex, as no relative humidity dependence is accounted for in the calculations. The DRF is largest when the aerosol is highest due to a combination of two factors. First, as the aerosol is moved to higher altitudes, there is a smaller proportion of scattering and absorbing atmosphere above the aerosol layer; thus more radiation is incident upon the aerosol (T_{at} in (2) increases). Second, and more important, as the BC is moved to higher altitudes, the aerosol layer moves above more cloudy layers in the atmosphere. As shown by *Haywood and Shine* [1997], BC that exists above cloud exerts a DRF that may be greater than that in clear skies by more than a factor of 10, the magnitude of the increase being a function of the cloud optical depth, the surface reflectance, and the solar zenith angle. The large sensitivity of the DRF to the altitude of the aerosol emphasizes the need to determine the vertical profile of the BC aerosol accurately. CW96 state that the chemical transport model tends to overaccumulate BC in the middle troposphere, which suggests that the DRF obtained from their climatology in the base case calculations may be too high. If it is assumed that BC is confined to the lowest 2 km of the atmosphere (i.e., there is negligible transport from the boundary layer into the free troposphere), then the DRF ranges from approximately +0.45 to +0.9 W m^{-2}, depending upon the vertical profile.

Table 3. Variation of Direct Radiative Forcing for Different Model Geometric Mean Radii for Black Carbon Aerosol

r_m, μm	Northern Hemisphere	Southern Hemisphere	Global
0.01	+1.71	+0.42	+1.06
0.0118	+1.70	+0.42	+1.06
0.05	+1.05	+0.25	+0.65
0.10	+0.61	+0.15	+0.38
0.50	+0.24	+0.06	+0.15

Unit of measure is W m^{-2}.

5.4. Sensitivity of the DRF to Total BC Burden

The BC climatology of CW96 is derived using the MOGUNTIA chemical transport model. *Liousse et al.* [1996] (LPCWE96) have also developed a BC climatology using the GRANTOUR chemical transport model and calculate the total global BC to be 0.13 Tg, which is 54% lower than the 0.28 Tg calculated by CW96. The optical parameters assumed by LPCWE96 (see their Table 2) clearly indicate that the BC modeled in their study is the optically active fine-particle BC, as these parameters are very similar to those shown in Figure 2. The BC climatology of LPCWE96 is not yet generally available. However, the spatial distribution of the BC is similar to that of CW96; thus, to a first approximation, the CW96 climatology may be scaled by a factor of 46% to represent the BC climatology of LPCWE96. Because of the uncertainty in the total column burden of BC, only a crude sensitivity study is possible at the current time. Calculations are performed in which the DRF of BC calculated from the CW96 climatology is scaled to the total atmospheric burden for BC atmospheric burdens ranging from 0.05 to 0.30 Tg. Additionally, because of

Table 4. Sensitivity Analysis of Direct Radiative Forcing (DRF) for Black Carbon (BC) Assuming Different Total Global Burdens and Different Vertical Profiles

Total Burden, Tg BC	DRF for Different Vertical Profiles, W m^{-2}			
	Cooke and Wilson [1996]	1 km	2.5 km	5 km
0.05	+0.19	+0.11	+0.14	+0.17
0.10	+0.38	+0.21	+0.27	+0.33
0.13*	+0.49*	+0.28*	+0.35*	+0.43*
0.15	+0.57	+0.32	+0.41	+0.50
0.20	+0.76	+0.43	+0.54	+0.66
0.25	+0.95	+0.54	+0.68	+0.83
0.28*	+1.06*	+0.60*	+0.76*	+0.93*
0.30	+1.14	+0.64	+0.81	+1.00

*Column burdens of black carbon and the associated radiative forcing for the *Liousse et al.* [1996] and *Cooke and Wilson* [1996] climatologies.

the importance of the altitude of the aerosol upon the DRF (see section 5.3), further sensitivity studies are performed assuming that the BC is confined to the lowest 1, 2.5, and 5 km. The DRF for BC shown in Figure 8 is used to approximate the DRF for BC aerosol confined to these layers by taking the DRF at the midaltitude of the aerosol layer. The results are shown in Table 4.

Table 4 shows that the DRF ranges from approximately +0.1 to +1.1 W m^{-2}, indicating that the uncertainty in the estimate is very large. A DRF of approximately +0.4 W m^{-2} is chosen as representative of the DRF due to BC with a factor of 3 uncertainty. The global mass of BC required to produce a DRF of +0.4 W m^{-2} assuming the same spatial distribution of the aerosol as CW96 is approximately 0.106 Tg. Because much of the uncertainty in the DRF due to BC is due to the uncertainty in the total global burden, the normalized DRF in W mg^{-1} is calculated; the range is approximately +1.1 to +1.9 W mg^{-1}. This range represents uncertaintics in the altitude of the aerosol alone, assuming that the BC aerosol is fine-particle BC (see section 5.2).

6. Results: External Mixture of Sulfate and BC Aerosol

To simulate the effects of an external mixture of sulfate and BC aerosol, the DRF for sulfate is simply added to that for BC. This approach is justified, as in general, the optical depth of the sulfate and BC aerosols is small, which means that any radiation scattered/absorbed by sulfate aerosol is unlikely to undergo scattering/absorption by the BC aerosol, and vice versa. The DRF for an external mixture of sulfate and BC is modeled using the base case DRF for sulfate and a global DRF of BC of +0.4 W m^{-2} with a factor of 3 uncertainty (see section 5.4). Figure 15 shows that the DRF due to an external mixture produces strongly contrasting regions of positive and negative DRF, the sign of the DRF being a strong function of the surface reflectance. The three regions where there is a positive DRF are over central Africa, the Tibetan plateau, and high latitudes of both hemispheres; these are regions where the surface albedo is relatively high.

The single scattering albedo is approximated by determining the annual average of the optical depth of both sulfate aerosol and BC aerosol. The BC is scaled to a mass of 0.106 Tg (section 5.4). The total column burden of the sulfate is determined and multiplied by the specific extinction at 92% relative humidity to determine the sulfate aerosol optical depth. This relative humidity is chosen in these calculations, as this is the fixed rela-

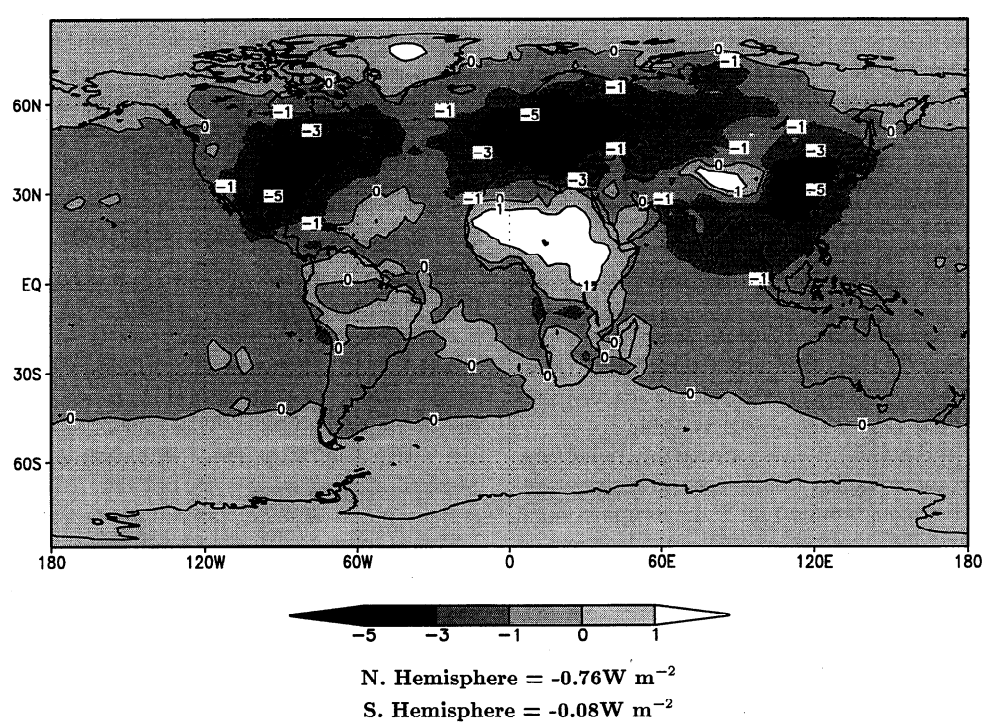

Figure 15. DRF (W m^{-2}) due to an external mixture of sulfate and BC aerosol using the climatology of KCS97 and scaling the climatology of CW96 as described in the text. The hemispheric mean DRFs are also shown.

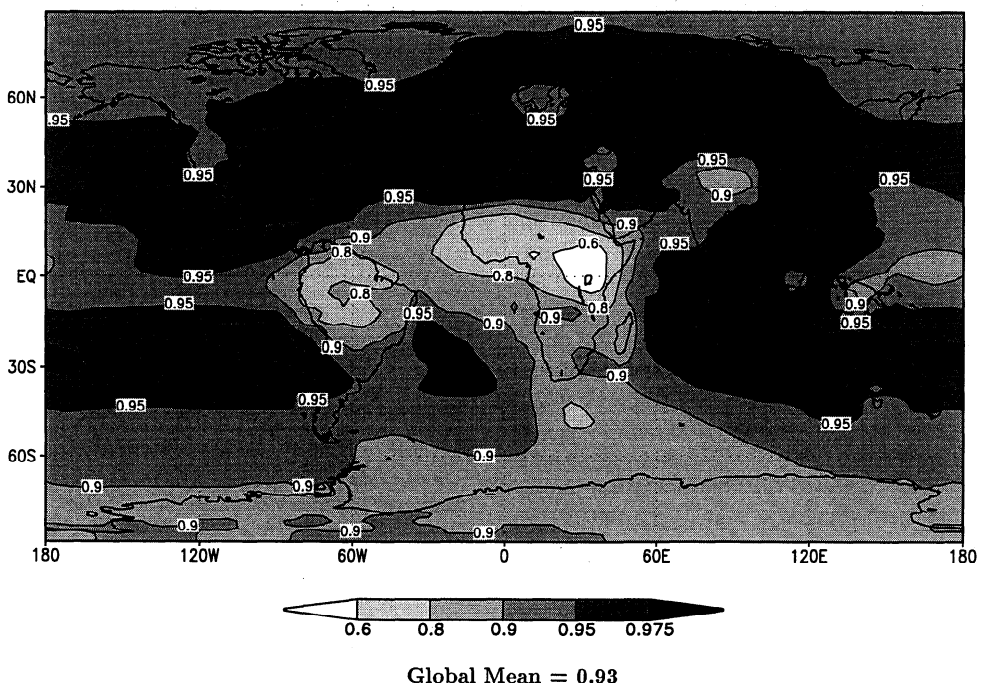

Figure 16. Single scattering albedo due to an external mixture of sulfate and BC aerosol using the climatology of KCS97 and scaling the climatology of CW96 as described in the text.

tive humidity necessary to produce the radiative forcing of the base case (see Table 1). The single scattering albedo may then be determined as

$$\omega_{\text{external}} = \frac{\omega_{\text{sul}}\tau_{\text{sul}} + \omega_{\text{BC}}\tau_{\text{BC}}}{\tau_{\text{sul}} + \tau_{\text{BC}}} \quad (4)$$

where τ_{sul} is the optical depth of the sulfate and τ_{BC} is the optical depth of the BC. The single scattering albedo at 0.55 μm derived using this method is shown in Figure 16. The global mean single scattering albedo is 0.93 but ranges from less than 0.5 in regions where the aerosol is predominantly BC (i.e., the areas where biomass burning occurs) to in excess of 0.975 in some industrialized regions of the northern hemisphere. In continental regions of the northern hemisphere, the single scattering albedo generally exceeds 0.95, although some areas of Scandinavia and the western United States have single scattering albedos of between 0.925 and 0.95.

When comparing the single scattering albedo from an external mixture of sulfate and BC with atmospheric measurements, there are three important caveats to consider. First, the single scattering albedo shown in Figure 16 does not include any sulfate from natural sources. Second, other aerosol types such as dust, organic carbon, and nitrates are not included in the calculations. Third, the effects of internal mixing are not included in the calculations. The first and second of these caveats mean that the single scattering albedo calculated using this method will be lower than observations, although the third cavcat may act to offset the first two to some extent. LPCWE96 has recently calculated the single scattering albedo of a composite mixture of sulfate, BC, and organic carbon and finds that the single scattering albedo at 0.55 μm ranges from 0.84 to 1.0, results that generally compared favorably with observations (see LPCWE96, Table 8), even though other aerosol particles such as dust and nitrates are not included. Inclusion of organic carbon aerosol in our calculations would result in a better agreement with observations.

A particular concern relating to the calculation of the global distribution and global mean single scattering albedos is that it is difficult to include the effects of relative humidity upon the optical depth of sulfate in a consistent manner. The global single scattering albedo of 0.93 reduces to 0.90 and 0.88 using the optical properties corresponding to relative humidities of 80% and 70%, respectively. This indicates that, when measurements of the single scattering albedo of a hygroscopic aerosol are made in situ in the atmosphere, it is important to make corresponding measurements of the relative humidity and incorporate these data in the results. It should also be noted that these calculations show column-averaged single scattering albedos. Recently, *Hansen et al.* [1997] used a simplified GCM to demonstrate that the critical single scattering albedo that determines when the DRF switches from a negative forcing to a positive forcing is a function of the horizontal and vertical spatial distribution of the applied partially absorbing aerosol due to surface albedo and cloud effects. The additional complexities of calculating a single scattering albedo of a mixture of hygroscopic sulfate aerosol and absorbing BC aerosol highlighted here further indicate the limitations of the concept of a global critical single scattering albedo and in the interpretation of such a concept for specific regions of the globe. These limitations and concerns are further discussed by *Heintzenberg et al.* [1997].

7. Discussion and Conclusions

The global mean DRF calculated for sulfate aerosol from the climatology of KCS97 is approximately -0.8 W m^{-2}; the global mean DRF from the climatology of LR91 is calculated as -0.6 W m ^{2}. These results may be compared to the global

mean DRFs of -0.28 W m^{-2} calculated by *Kiehl and Briegleb* [1993], -0.95 W m^{-2} calculated by *Taylor and Penner* [1994], -0.29 W m^{-2} calculated by *Boucher and Anderson* [1995], and -0.38 W m^{-2} calculated by *Haywood et al.* [1997a]. *Houghton et al.* [1995] suggest a DRF due to sulfate aerosol of approximately -0.4 W m^{-2} with a factor of 2 uncertainty. Thus the DRF of anthropogenic sulfate calculated in this study is rather higher than in many recent studies, with differences occurring due to different aerosol climatologies, assumed vertical profiles of the aerosol, aerosol size distributions, radiation codes, GCMs, and treatments of relative humidity. These differences mean that it is very difficult to determine exactly why differences in the DRF due to sulfate occur. While there has been a comprehensive intercomparison of the DRF due to sulfate aerosol using column models and multispectral radiation codes (O. Boucher et al., submitted paper, 1997), only when a similar intercomparison project for global distributions of sulfate has been performed will it be possible to reconcile the DRFs from each global modeling study.

The lack of representation of a diurnal cycle in the GFDL R30 GCM means that an average solar zenith angle must be used in the DRF calculations. Analysis of column DRF calculations from the recent study of O. Boucher et al. (submitted paper, 1997) suggests that the instantaneous global clear-sky DRF due to sulfate will be overestimated when using an average solar zenith angle by as much as 25%, assuming a global aerosol optical depth of 0.10 and a surface reflectance of 0.15. However, the main features from the sensitivity studies that are presented in this study are unlikely to change due to this limitation of the model. This deficiency in the calculations of the DRF is small in the case of BC aerosol, as the DRF is a much less complex function of solar zenith angle [*Haywood and Shine*, 1997], as the primary physical process that determines the DRF for BC is absorption rather than scattering.

Additionally, it is possible that the calculated values for the sulfate DRF may be too high due to the lack of representation of subgrid-scale cloud amount at high relative humidities by the on/off cloud scheme contained within the GFDL R30 GCM. Note that even the GCM studies of *Boucher and Anderson* [1995] and *Haywood et al.* [1997a] that contain subgrid-scale cloud fractions do not consider the correlation between subgrid-scale cloudy areas and areas of high relative humidity.

The DRF calculated for BC aerosol from the climatology of CW96 is approximately $+1.1$ W m^{-2}; this is considered to be an approximate upper bound for the DRF due to the relatively high BC loading and to the overaccumulation of BC in the upper troposphere by the MOGUNTIA model. The sensitivity study of section 5.4 shows that a DRF of $+0.4$ W m^{-2} with a factor of 3 uncertainty appears reasonable. This value is in reasonable agreement with the $+0.20$ W m^{-2} calculated by *Haywood et al.* [1997a] for fossil-fuel BC if one considers that approximately 60% of the BC in the CW96 climatology is of fossil-fuel origin. At this time, the global burden of optically active fine-particle BC remains highly uncertain. Because of this, a more satisfactory way of presenting the DRF due to BC is the normalized DRF, which is calculated to range from $+1.1$ to $+1.9$ W mg^{-1}. The uncertainty in this estimate is due solely to uncertainties in the vertical profile of the BC aerosol if one assumes fine-particle BC. The most obvious discrepancy that needs to be addressed in future estimates of the DRF due to BC is the differences in the total BC loading between CW96 and LPCWE96; uncertainties in the vertical distribution and size distributions of BC particles also need to be addressed.

The vertical profile of both aerosol species has been shown to be very important in determining the overall DRF of both aerosol species, with sulfate at low altitudes giving the strongest DRF due to the effects of relative humidity. BC at high altitudes gives the strongest DRF as the aerosol is moved above the cloudy layers of the atmosphere. These results suggest that chemical transport models must simulate the vertical profile of each aerosol species accurately; improved parameterizations for deep convection and increased vertical resolution in the chemical transport models are desirable. Recently, *Chylek et al.* [1996] found that the concentrations of BC over southern Nova Scotia were higher at altitudes of 1–3 km than those below 1 km, suggesting that BC aerosol does indeed become somewhat lofted and may exist within or above clouds. The recent Tropospheric Aerosol Radiative Forcing Experiment (TARFOX) measurement campaign over the Atlantic Ocean off the eastern coast of the United States found that the single scattering albedo was highest close to the surface and decreased with altitude due to the combined effects of elevated carbon to sulfate ratios at higher altitudes and relative humidity effects (P. Hobbs, personal communication, 1997). Additionally, the effects of BC emitted directly in the upper troposphere by aircraft are not considered in the study of either CW96 or LPCWE96; the long residence time and the elevation of the BC mean that this source of BC in the troposphere should be considered in future chemical transport models. Additional measurements of the vertical profile of both sulfate and BC are needed to provide data for chemical transport model verification, so that the DRF of both species of aerosol may be better constrained.

Adopting the global DRF from the base case for sulfate aerosol (-0.8 W m^{-2}) and a value of $+0.4$ W m^{-2} for the BC DRF leads to a global DRF for an external mixture of -0.4 W m^{-2}. This indicates that, in this model, the DRF due to sulfate is reduced by 50% due to the presence of BC aerosol. However, it should also be noted here that further components of anthropogenic aerosols also need to be considered in calculating the overall direct effect of anthropogenic aerosols, these components being organic carbon, dust, and nitrates [*Houghton et al.*, 1996].

A further issue that is not investigated in this study is that of the degree and type of mixing between aerosol species. The GCM calculations of *Haywood et al.* [1997a] suggest that internally mixed sulfate and BC aerosols should exert a DRF that is more positive than an external mixture of the same chemical composition. The calculations presented in this study represent an external mixture; thus, when internally mixed, the BC may exert a more positive forcing than that modeled here.

This study shows that, although considerable attention has been given to modeling the radiative forcing of sulfate aerosol and the subsequent climate response, the direct radiative forcing due to sulfate aerosol remains uncertain due primarily to uncertainties in the total atmospheric burden, vertical profile of the aerosol, and treatment of relative humidity effects. Additionally, as in the work by *Haywood et al.* [1997a], the DRF of BC may be significantly higher than previous estimates [e.g., *Haywood and Shine*, 1995; *Chylek et al.*, 1995] due to BC aerosol residing above and within clouds. Further measurements of the vertical profile of both aerosol species are critical if the overall climatic influence of the two species is to be accurately assessed.

Acknowledgments. The authors would like to thank Prasad Kasibhatla and J. Langner and H. Rodhe for providing the sulfate aerosol climatologies, and William Cooke for providing the black carbon climatology. Stuart Freidenreich is thanked for providing the new short wave radiation code. Two anonymous referees are also thanked for their useful comments.

References

Berner, A., S. Sidla, Z. Galambos, C. Kruisz, R. Hitzenberger, H. M. ten Brink, and G. P. A. Kos, Modal character of atmospheric black carbon size distributions, *J. Geophys. Res.*, *101*, 19,559–19,565, 1996.

Boucher, O., and T. L. Anderson, GCM assessment of the sensitivity of direct climate forcing by anthropogenic sulfate aerosols to aerosol size and chemistry, *J. Geophys. Res.*, *100*, 26,117–26,134, 1995.

Boucher, O., and U. Lohmann, The sulfate-CCN-cloud albedo effect: A sensitivity study with two general circulation models, *Tellus*, *Ser. B*, *47*, 281–300, 1995.

Charlson, R. J., J. Langner, H. Rodhe, C. B. Leovy, and S. G. Warren, Perturbation of the northern hemisphere radiative balance by backscattering from anthropogenic sulfate aerosols, *Tellus*, *Ser. AB*, *43*, 152–163, 1991.

Chylek, P., and J. Wong, Effect of absorbing aerosols of global radiation budget, *Geophys. Res. Lett.*, *22*, 929–931, 1995.

Chylek, P., V. Ramaswamy, and R. J. Cheng, Effect of graphitic carbon on the albedo of clouds, *J. Atmos. Sci.*, *41*, 3076–3084, 1984.

Chylek, P., V. Srivastava, R. G. Pinnick, and R. T. Wang, Scattering of electromagnetic waves by composite spherical particles: Experiments and effective medium approximations, *Appl. Opt.*, *27*, 2936–2404, 1988.

Chylek, P., G. Videen, and D. Ngo, Effect of black carbon on the optical properties and climate forcing of sulfate aerosols, *J. Geophys. Res.*, *100*, 16,325–16,332, 1995.

Chylek, P., C. M. Banic, B. Johnson, P. A. Damiano, G. A. Isaac, W. R. Leaitch, P. S. K. Liu, F. S. Boudala, B. Winter, and D. Ngo, Black carbon: Atmospheric concentrations and cloud water content measurements over southern Nova Scotia, *J. Geophys. Res.*, *101*, 29,105–29,110, 1996.

Cooke, W. F., and J. J. N. Wilson, A global black carbon model, *J. Geophys. Res.*, *101*, 19,395–19,409, 1996.

Fassi-Fihri, A., K. Suhre, and R. Rosset, Internal and external mixing in atmospheric aerosols by coagulation: Impact on the optical and hygroscopic properties of the sulphate-soot system, *Atmos. Environ.*, *31*, 1393–1402, 1997.

Fitzgerald, J. W., Approximation formulas for the equilibrium size of an aerosol particle as a function of its dry size and composition and the ambient relative humidity, *J. Appl. Meteorol.*, *14*, 1044–1049, 1975.

Freidenreich, S. M., and V. Ramaswamy, A new multi-band solar radiative parameterization, in *Ninth Conference on Atmospheric Radiation, February 2–7, Long Beach, California*, pp. 129–130, Am. Meteorol. Soc., Boston, Mass., 1997.

Hansen, J., M. Sato, and R. Reudy, Radiative forcing and climate response, *J. Geophys. Res.*, *102*, 6831–6864, 1997.

Haywood, J. M., and K. P. Shine, The effect of anthropogenic sulfate and soot aerosol on the clear sky planetary radiation budget, *Geophys. Res. Lett.*, *22*, 603–606, 1995.

Haywood, J. M., and K. P. Shine, Multi-spectral calculations of the radiative forcing of tropospheric sulphate and soot aerosols using a column model, *Q. J. R. Meteorol. Soc.*, *123*, 1907–1930, 1997.

Haywood, J. M., D. L. Roberts, A. Slingo, J. M. Edwards, and K. P. Shine, General circulation model calculations of the direct radiative forcing by anthropogenic sulphate and fossil-fuel soot aerosol, *J. Clim.*, *10*, 1562–1577, 1997a.

Haywood, J. M., R. J. Stouffer, R. T. Wetherald, S. Manabe, and V. Ramaswamy, Transient response of a coupled model to estimated changes in greenhouse gas and sulfate concentrations, *Geophys. Res. Lett.*, *24*, 1335–1338, 1997b.

Haywood, J. M., V. Ramaswamy, and L. J. Donner, A limited-area-model case study of the effects of subgrid-scale variations in relative humidity and cloud upon the direct radiative forcing of sulfate aerosol, *Geophys. Res. Lett.*, *24*, 143–146, 1997c.

Heintzenberg, J., R. J. Charlson, A. D. Clarke, C. Liousse, V. Ramaswamy, K. P. Shine, and M. Wendisch, Measurement and modelling of aerosol single-scattering albedo: Progress, problems and prospects, *Contrib. Atmos. Phys.*, *70*, 249–264, 1997.

Horvath, H., Atmospheric light absorption—A review, *Atmos. Environ.*, *27*, Part A, 293–317, 1993.

Houghton, J. T., M. Filho, L. G. Callander, N. Harris, A. Kattenberg, and K. Maskell (Eds.), *Climate Change 1995: The Science of Climate Change*, Cambridge Univ. Press, New York, 1996.

Jones, A., and A. Slingo, Predicting cloud-droplet effective radius and indirect sulphate aerosol forcing using a general circulation model, *Q. J. R. Meteorol. Soc.*, *122*, 1573–1595, 1996.

Jones, A., D. L. Roberts, and A. Slingo, A climate model study of the indirect radiative forcing by anthropogenic sulphate aerosols, *Nature*, *370*, 450–453, 1994.

Kasibhatla, P., W. L. Chameides, and J. St. John, A three-dimensional global model investigation of the seasonal variation in the atmospheric burden of anthropogenic sulfate aerosols, *J. Geophys. Res.*, *102*, 3737–3759, 1997.

Kiehl, J. T., and B. P. Briegleb, The relative roles of sulfate aerosols and greenhouse gases in climate forcing, *Science*, *260*, 311–314, 1993.

Langner, J., and H. Rodhe, A global three-dimensional model of the tropospheric sulfur cycle, *J. Atmos. Chem.*, *13*, 225–263, 1991.

Liousse, C., J. E. Penner, C. Chuang, J. J. Walton, and H. Eddleman, A global three-dimensional model study of carbonaceous aerosols, *J. Geophys. Res.*, *101*, 19,411–19,432, 1996.

McClatchey, R. A., R. W. Fenn, J. E. A. Selby, P. E. Volz, and J. S. Garing, Optical properties of the atmosphere, 3rd ed., *Pap. 411*, *Air Force Cambridge Res. Lab.*, Hanscom Air Force Base, Mass., 1972.

Meehl, G. A., W. M. Washington, D. J. Erickson III, B. P. Briegleb, and P. J. Jaumann, Climate change from increased CO_2 and direct and indirect effects of sulfate aerosols, *Geophys. Res. Lett.*, *23*, 3755–3758, 1996.

Mitchell, J. F. B., T. C. Johns, J. M. Gregory, and S. F. B. Tett, Climate response to increasing levels of greenhouse gases and sulphate aerosols, *Nature*, *376*, 501–504, 1995.

Nemesure, S., R. Wagener, and S. E. Schwartz, Direct shortwave forcing of climate by anthropogenic sulfate aerosol: Sensitivity to particle size, composition, and relative humidity, *J. Geophys. Res.*, *100*, 26,105–26,116, 1995.

Parungo, F., B. Kopcewicz, C. Nagamoto, R. Schell, P. Sheridan, C. Zhu, and J. Harris, Aerosol particles in the Kuwait oil fire plumes: Their morphology, size distribution, chemical composition, transport, and potential effect upon climate, *J. Geophys. Res.*, *97*, 15,867–15,882, 1992.

Parungo, F., C. Nagamoto, M. Y. Zhou, A. D. A. Hansen, and J. Harris, Aeolian transport of aerosol black carbon from China to the ocean, *Atmos. Environ.*, *28*, 3251–3260, 1994.

Penner, J. E., R. E. Dickinson, and C. A. O'Neill, Effects of aerosol from biomass burning on the global radiation budget, *Science*, *256*, 1432–1433, 1992.

Penner, J. E., C. S. Atherton, and T. E. Graedel, Global emissions and models of photochemically active compounds, in *Global Atmospheric Biospheric Chemistry*, edited by R. Prinn, pp. 223–248, Plenum, New York, 1994.

Pham, M., J. F. Muller, G. Brasseur, C. Granier, and G. Megie, A three-dimensional study of the tropospheric sulfur cycle, *J. Geophys. Res.*, *100*, 26,061–26,092, 1995.

Pilinis, C., S. N. Pandis, and J. H. Seinfeld, Sensitivity of direct climate forcing by atmospheric aerosols to aerosol size and composition, *J. Geophys. Res.*, *100*, 18,739–18,754, 1995.

Ramaswamy, V., and S. M. Freidenreich, Solar radiative line-by-line determination of water vapour absorption and water cloud extinction in inhomogeneous atmospheres, *J. Geophys. Res.*, *96*, 9133–9157, 1991.

Shettle, E. P., and R. W. Fenn, Models for the aerosols of the lower atmosphere and the effects of humidity variations on their optical properties, *Pap. AFGL-TR-79-0214*, Air Force Geophys. Lab., Bedford, Mass., 1979.

Slingo, A., A GCM parameterization for the shortwave radiative properties of water clouds, *J. Atmos. Sci.*, *46*, 1419–1427, 1989.

Tang, I. N., W. T. Wong, and H. R. Munkelwitz, The relative importance of atmospheric sulfates and nitrates in visibility reduction, *Atmos. Environ.*, *15*, 2463–2471, 1981.

Taylor, K., and J. E. Penner, Response of the climate system to atmospheric aerosols and greenhouse gases, *Nature*, *369*, 734–737, 1994.

Tegen, I., A. A. Lacis, and I. Fung, The influence of mineral aerosols from disturbed soils on climate forcing, *Nature*, *380*, 419–422, 1996.

Toon, O. B., J. B. Pollack, and B. N. Khare, The optical constants of

several atmospheric aerosol species: Ammonium sulphate, aluminium oxide and sodium chloride, *J. Geophys. Res.*, *81*, 5733–5748, 1976.

Twomey, S. A., The influence of pollution on the short-wave albedo of clouds, *J. Atmos. Sci.*, *34*, 1149–1152, 1977.

Waggoner, A. P., A. J. Vanderpol, R. J. Charlson, S. Larsen, L. Granat, and C. Tragardh, Sulphate-light scattering ratio as an index of the role of sulphur in tropospheric optics, *Nature*, *261*, 120–122, 1976.

Waggoner, A. P., R. E. Weiss, N. C. Ahlquist, D. S. Covert, S. Will, and R. J. Charlson, Optical characteristics of atmospheric aerosols, *Atmos. Environ.*, *15*, 1891–1909, 1981.

World Climate Program, *A Preliminary Cloudless Standard Atmosphere for Radiation Computation*, World Meteorol. Organ., Geneva, 1986.

Weast, R. C., 1987. Physical constants of inorganic compounds, in *CRC Handbook of Chemistry and Physics: 68th edition*, Weast, R. C. (ed), B67–146, CRC Press, Boca Raton.

Wetherald, R. T., and B. Soden, General simulation of atmospheric temperature and moisture in the GFDL AMIP experiment, Proceedings of the First International AMIP Scientific Conference, WCRP-92, *Rep. WMO/TD 732*, pp. 97–100, World Meteorol. Organ., Geneva, 1995.

J. M. Haywood, Met Research Flight, DERA, Farnborough, Hents GU14 0LX, England. (e-mail: jmhaywood@meto.gov.uk)

V. Ramaswamy, GFDL, Princeton University, Forrestal Campus, U. S. Route 1, Princeton, NJ 08542.

(Received June 20, 1997; revised October 29, 1997;
accepted November 19, 1997.)